Applied Surface Science 267 (2013) 164–168

Contents lists available at SciVerse ScienceDirect

Applied Surface Science

journal homepage: www.elsevier.com/locate/apsusc

# Decay of photo-induced conductivity in Sb-doped $SnO_2$ thin films, using monochromatic light of about bandgap energy

E.A. Floriano[a,b], L.V.A. Scalvi[a,*], J.R. Sambrano[c], A. de Andrade[d]

[a] Physics Dept. – FC, UNESP, São Paulo State University, Bauru, SP, Brazil
[b] Post-graduate Program in Science and Technology of Materials, UNESP, SP, Brazil
[c] Mathematics Dept. – FC, UNESP, Bauru, SP, Brazil
[d] Chemistry Dept., UNESP, Bauru, SP, Brazil

ARTICLE INFO

*Article history:*
Available online 19 September 2012

*Keywords:*
Tin dioxide
Electronic structure
Electrical conductivity
Sol–gel
Thin films

ABSTRACT

Doping tin dioxide ($SnO_2$) with pentavalent $Sb^{5+}$ ions leads to an enhancement in the electrical conductivity of this material, because $Sb^{5+}$ substitutes $Sn^{4+}$ in the matrix, promoting an electronic density increase in the conduction band, due to the donor-like nature of the doping atom. Results of computational simulation, based on the Density Functional Theory (DFT), of $SnO_2$:4%Sb and $SnO_2$:8%Sb show that the bandgap magnitude is strongly affected by the doping concentration, because the energy value found for 4 at%Sb and 8 at%Sb was 3.27 eV and 3.13 eV, respectively, whereas the well known value for undoped $SnO_2$ is about 3.6 eV. Sb-doped $SnO_2$ thin films were obtained by the sol–gel-dip-coating technique. The samples were submitted to excitation with below theoretical bandgap light (450 nm), as well as above bandgap light (266 nm) at low temperature, and a temperature-dependent increase in the conductivity is observed. Besides, an unusual temperature and time dependent decay when the illumination is removed is also observed, where the decay time is slower for higher temperatures. This decay is modeled by considering thermally activated cross section of trapping centers, and the hypothesis of grain boundary scattering as the dominant mechanism for electronic mobility.



## 1. Introduction

Many applications, including optical and electronic devices, have been reported for tin dioxide ($SnO_2$), which is a wide bandgap (about 3.6 eV) semiconductor [1] of tetragonal structure of rutile type. In the form of thin film, it presents high transparency in the visible range and high reflectivity in the infrared [2]. Its processing normally gives birth to defects such as oxygen vacancies and interstitial tin atoms, which act as donors in the $SnO_2$ matrix, increasing the electron density in the conduction band, leading to fair n-type conduction [3]. Doping this non-stoichiometric compound with antimony strongly modifies its intrinsic free carrier concentration. The resistivity of Sb-doped thin films decreases as the doping degree increases until about 8 at%. However, the resistivity increases for higher Sb doping [4], which suggests a limit for simple substitutional incorporation along with microstructure phenomena. The resistivity decrease for lower Sb incorporation is related to the free carrier concentration increase, coming from the replacing of $Sn^{4+}$ by $Sb^{5+}$ ions, which acts as donor-like centers in the $SnO_2$ lattice. For high doping levels, the increase of resistivity is either related to the presence of an increasing amount of $Sb^{3+}$ giving rise to acceptor levels trapping the intrinsic electrons [5] or by Sb segregation at particle surface [6,7]. XAS data reveals that the antimony are mostly in the oxidation state +5, in substitutional sites located near grain boundary surface region [7,8]. The increase of Sb concentration also increases the oxygen vacancy concentration close to the $Sb^{5+}$ ion, which lowers the grain boundary potential barrier.

The aim of this paper is to evaluate theoretically the electronic band structure for Sb-doped $SnO_2$ and to test the obtained parameters with a experimental characterization of the decay of photo-excited conductivity, using monochromatic light sources with energy below and above the theoretically evaluated bandgap energy, showing a combination of theory and experiment.

The knowledge of optically excited electrical characteristics in Sb-doped $SnO_2$ is fundamental for design and operation of optoelectronic devices. The optical ionization of Sb-related defects and the analysis of charge trapping back help this investigation, since it combines optical and electrical properties of Sb-doped $SnO_2$ thin films. Recombination of electron–hole pairs with desorbed oxygen species leads to persistent photoconductivity (PPC) effect in undoped $SnO_2$ sol–gel thin films at low temperature [9]. The investigation in the range 250–350 K, reported here, shows a small, but measurable decay of the conductive metastable state in Sb-doped $SnO_2$ thin films, after removing the illumination.

* Corresponding author.
*E-mail address:* scalvi@fc.unesp.br (L.V.A. Scalvi).

0169-4332/$ – see front matter © 2012 Elsevier B.V. All rights reserved.
http://dx.doi.org/10.1016/j.apsusc.2012.09.003

## 2. Experimental

The desired amount of $SbF_3$ was added to an aqueous solution of $SnCl_4{\cdot}5H_2O$ (0.5 mol $l^{-1}$), under stirring with a magnetic bar, followed by addition of $NH_4OH$ until pH reaches 11. Ions $Cl^-$ and $NH_4^+$ were eliminated by dialysis. Films were deposited on silicate glass substrates by dip-coating with 10 cm/min dip rate. Multi-dipped films were continuously deposited at room temperature with firing at 400 °C for 10 min after each dip. Resulting film (10 layers) was annealed at 550 °C for 1 h. The resulting thickness was evaluated from scanning electron microscopy as well from the interference fringes of the transmittance spectra [10], yielding about 240 nm. This value is in good agreement with previously evaluated samples deposited by the same method, either by SEM as well as X-ray reflectometry [11].

In (indium) electrodes were deposited on the samples by resistive evaporation technique, through a shadow mask in an Edwards Auto 500 evaporator system. Electrodes are annealed to 150 °C by 30 min at room atmosphere. Low temperature measurements were done in a He-closed cycle Janis Cryostat in the range 10–350 K. For the decay of photo-induced conductivity, samples were irradiated either with a LED (InGaN) with average wavelength of 450 nm (below the theoretically evaluated bandgap energy) and average power of 15 mW, or with the fourth harmonic of a Nd:YAG pulsed laser, with 266 nm (above the bandgap light) of wavelength, 4.8 mW of power and frequency of 10 Hz. The decay of photo-excited conductivity is experimentally applied to $SnO_2$:4 at%Sb, in order to understand the electron trapping phenomena for this kind of sample. The experiment is carried out as follows: the irradiation with above bandgap energy may create electron–hole pairs and ionize intra-bandgap defects, such as substitutional $Sb^{5+}$, grain boundary located $Sb^{3+}$ and oxygen vacancies. On the other hand, the below bandgap light source does not generate electron–hole pairs. After removing the illumination, the time–temperature dependence of charge carrier trapping by defects is measured and the thermally activated capture cross section of the dominating level is evaluated.

## 3. Band structure numerical simulation

The computational simulations of bulk $SnO_2$:4 at%Sb and $SnO_2$:8 at%Sb was developed with the CRYSTAL06 program [12], applying the Density Functional Theory (DFT) [13], with the hybrid functional B3LYP [14]. Sn and O centers have decried in schemes [DB]-21G and DB-31G [15], respectively. DB concerns the Durand–Barthelat [16] non relativistic large effective core pseudopotential. The Sn and O centers were described by the 6-31G [15] and 6-31G [16] all-electron basis set, respectively. For the Sb atom, it was used original all-electron basis set proposed by Towler [17].

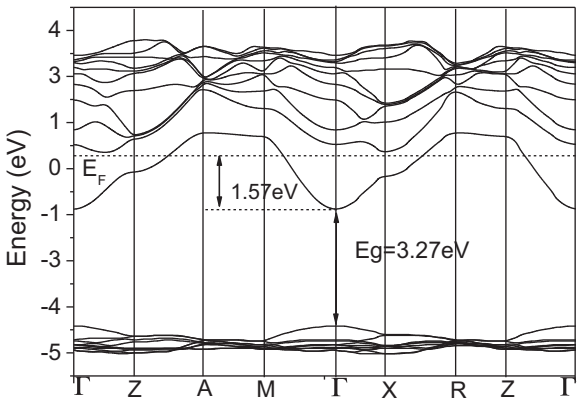


**Fig. 1.** Band structure diagram, evaluated for bulk in $SnO_2$:4 at%Sb.

Tin dioxide, when crystallized in the rutile tetragonal structure, presents tetragonal symmetry $D_{4h}^{14}$ (spatial group $P4_2/mnm$), with two Sn atoms and four O atoms unit cell. It is characterized by two lattice parameters $a$ and $c$ and by the internal coordinate $u$. For the simulation of $SnO_2$:4%Sb, it has been used a super cell (72 atom) $2 \times 3 \times 2$, obtained from the $SnO_2$ unit cell, using experimental rutile structural parameters: $a = 4.737$ Å, $c = 3.186$ Å and internal parameter $u = 0.306$ [18]. The band structure calculation of $SnO_2$:4 at%Sb and $SnO_2$:8 at%Sb were submitted to geometrical optimization process of atomic positions.

## 4. Results and discussion

### 4.1. Band structure calculation

Fig. 1 presents the band structure energy for bulk $SnO_2$:4 at%Sb, where $E_F$ corresponds to the Fermi level energy. This diagram shows that the valence band top and the conduction band bottom are located at $\Gamma$ direction, indicating that the band transition is of direct type in this $\Gamma$ direction, with a bandgap of 3.27 eV. The same analysis for $SnO_2$:8 at%Sb (not shown) shows that the bandgap magnitude depends on the doping concentration, because the energy value for 8 at%Sb is 3.13 eV. Both values are rather lower, when compared to calculated undoped material (3.6 eV) suggesting that the presence of $Sb^{5+}$, substituting $Sn^{4+}$ ions in the matrix, promotes a bandgap decrease. Besides, it shifts the Fermi level for a position well above the conduction band bottom, and the difference between the Fermi level and the conduction band bottom is 1.57 eV

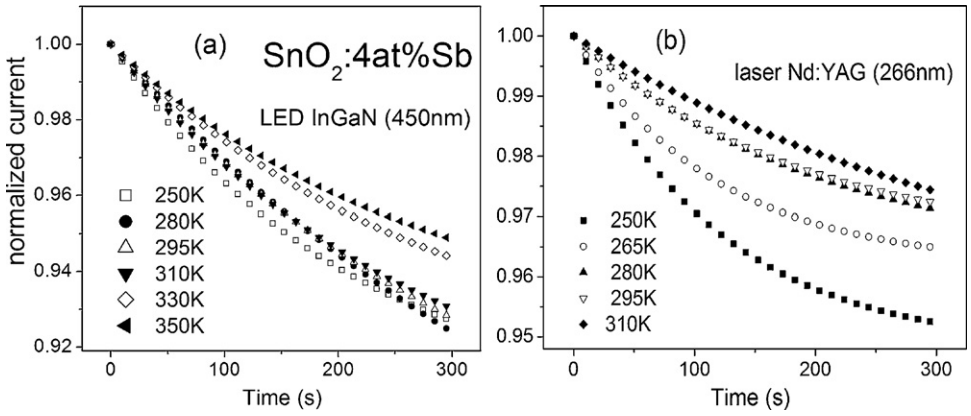


**Fig. 2.** Decay of photo-induced current for several temperatures to $SnO_2$:4 at%Sb thin film after irradiation with (a) InGaN LED (450 nm), (b) Nd:YAG laser (266 nm).

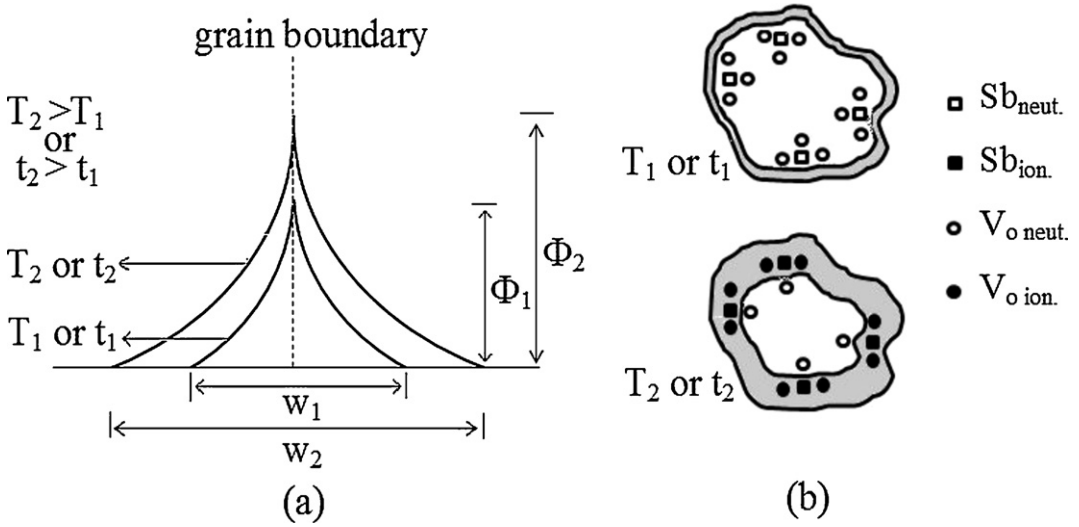


**Fig. 3.** (a) Potential barrier ($\phi$) and grain boundary depletion layer width ($W$) variation with temperature and time. (b) Grain diagram at $t = 0$, showing the depletion layer width (up), and grain diagram for long time, showing the electron capture by oxygen vacancies ($V_O$) and Sb ions, which become located inside the grain depletion layer (down).

and 1.93 eV for $SnO_2$: doped with 4 at%Sb and 8 at%, respectively. The very high concentration of Sb ions promotes the degenerescency of energy levels and, thus, the Fermi level is raised to above the conduction band minimum. This result is in good agreement with the expected one for semiconductors with very high doping level.

### 4.2. Decay of photo-induced conductivity

Normalized conductivity decay as function of time is shown in Fig. 2 for $SnO_2$:4 at%Sb film, after the film is excited by the LED blue light (450 nm), for 300 s of recorded data (Fig. 2(a)). In this case, the light energy is lower than the evaluated bandgap energy (Fig. 1). Fig. 2(b) shows the same sort of data, using the 4th harmonic of a Nd:YAG laser (266 nm) as light source. It is easily seen that after irradiation removal in both cases, the magnitude of the decay is temperature dependent. Unexpectedly, the decay becomes slower as the temperature increases, in opposition to previously reported results for Er-doped [9] and Eu-doped $SnO_2$ [19], when the same above bandgap light source was used (4th harmonic of Nd:YAG laser) and also in apparent contradiction with the expected increase in the electron trapping rate with temperature increase. Although one may suppose that it is a result induced by the below bandgap light source, the result shown in Fig. 2(b) discharge that possibility, and leads to the conclusion that it is a result of the Sb-doped $SnO_2$ film itself. Then, the PPC phenomena observed at low temperature (mainly at 70 K) [20], is not expected for this sort of sample. Although there is some overlapping in the data for longer times, the average results are a clear indication of this behavior. For instance, comparing data for 250 K and 350 K, with LED excitation, at 300 s, the optically excited electrical current decays about 8% of its initial value at 250 K,whereas at 350 K it decays only 6% of its initial value. Fig. 2(b) (laser excitation) shows similar data. The decay is also light source dependent, because comparing same temperatures, the laser excitation led to slower decay when compared to LED excitation. Although these temperature and light source dependencies are clearly observed in Fig. 2, the values are actually rather close, and some overlapping, mainly at the beginning of the decay is observed. This may be an indication that competing mechanisms are taking place: besides the electron trapping by distinct thermally activated centers, the mobility, which is temperature dependent, may also be time dependent, as will be discussed below.

In order to model the decay, the resistance as function of time, for a fixed temperature is given by:

$$R(t) = [K_s \cdot n(t) \cdot \mu(t) \cdot q]^{-1} \quad (1)$$

where $K_s$ is a constant, $n(t)$ is the time dependent electron concentration, $\mu(t)$ is the time dependent electronic mobility and $q$ is the electron charge.

The observed decay of conductivity as function of time means that the resistance of the film increases with time. The decay of photo-induced electrons ($n$) from the conduction band to the trapping defect is given by a simple differential equation [21], whose solution was previously published [9,21]. Considering that mobility ($\mu$) is dominated by the grain boundary scattering, we may neglect bulk scattering mechanisms (phonon and ionized impurity). X-ray diffraction data for these films (not shown) exhibits a diffuse shape profile, typical of small crystallite domain. The average crystallite size evaluate from line broadening XRD pattern is about 5–8 nm [7]. Then, electrical transport, dominated by grain boundary scattering, is an adequate hypothesis, since the grain size is very small. The mobility due to grain boundary scattering is proportional to $T^{-1/2} \cdot \exp(-\phi \cdot k^{-1}T^{-1})$ [22], where $\phi$ is the grain boundary potential barrier. Substituting these definitions into time-dependent resistance, one obtains:

$$R(t) = \frac{K_R}{q \cdot n \cdot \mu} = C_x + \frac{K_R \cdot T \cdot ((3k)/m^*)^{1/2} \cdot \gamma_\infty \cdot \exp(-((E_{cap} - \phi)/(kT))) \cdot t}{A \cdot q} \quad (2)$$

where $K_R$ is the proportionality constant between resistivity and resistance and $A$ is the grain boundary scattering constant [22]. $C_x$ is temperature dependent but not time dependent [9]. $\gamma_n = \gamma_\infty \cdot \exp(-E_{cap}/kT)$ is the capture cross section, $E_{cap}$ is the potential barrier for electron trapping and $\gamma_\infty$ is the constant capture cross section (infinite temperature). Eq. (2) means that $R(t)$ must be a linear function of time for fixed temperature. Evaluating the first derivative and calling it as *slope*, it is obtained:

$$\frac{dR}{dt} = slope = K_f \cdot T \cdot \exp\left[-\frac{E_{cap} - \phi}{kT}\right] \quad (3)$$

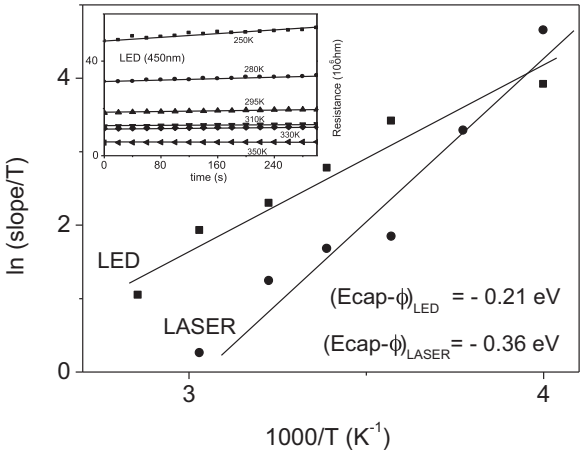


**Fig. 4.** Plot of ln(*slope*/*T*) as function of reciprocal temperature, according to theory shown in this paper for $SnO_2$ doped with 4 at%Sb. Inset: resistance as function of time data and linear regression for several temperatures, after irradiation with the InGaN LED.

where $K_f$ is $\gamma_\infty \cdot (3\,k/m^*)^{1/2} \cdot K_R/(A \cdot q)$. Therefore a plot of ln(*slope*/*T*) as function of $1/T$ yields the quantity $(E_{cap} - \phi)$ directly from the curve inclination.

Taking into account the temperature dependence of the capture cross section ($\gamma_n$), it is expected that a capture rate increase with the temperature increase, as reported for other thermally activated defects [9,19,21]. In order to explain the unusual results of Fig. 2, one must think on the temperature and time dependence of mobility. Fig. 3 represents the time and temperature dependency of the barrier height concomitant with boundary layer depletion layer. The increase in the barrier height with temperature is in good agreement with reported data for $SnO_2$ [23]. Although the mobility decreases with temperature increase, the effect of ionizing more defects with light irradiation, besides the statistical electron density, at higher temperatures compensates the mobility influence and the overall result is a higher conductivity for higher temperature (not shown in Fig. 2, since the plotted current is normalized, but it will be recalled next paragraph). This temperature influence may be associated with growth of the barrier height and depletion layer between grains, as represented in Fig. 3. A similar effect may be used to explain the time dependence: $Sb^{5+}$ ions are located preferentially at substitutional sites close to the grain boundary layer, surrounded by oxygen vacancies [7], as also sketched in Fig. 3. Considering that these are the main trapping defects (ionized oxygen vacancies and ionized Sb atoms – both donors in $SnO_2$), as the time passes the trapping increases the barrier height and depletion layer width, and, in this case, it is more effective for higher temperatures due to the thermal influence in the grain boundary mobility, as already discussed. Then, the mobility influence in the time dependent conductivity seems to be more effective as the temperature increases, overwhelming the electron capture rate, which explain the temperature dependency on the observed conductivity decay.

A plot of $\ln(slope/T) \times T^{-1}$ curves, in accordance with Eq. (3), is shown in Fig. 4 for $SnO_2$:4 at%Sb, which allows obtaining the quantity $(E_{cap} - \phi)$. A plot of resistance as function of time is shown in the inset of Fig. 4, for several measured temperatures, for LED excitation. The linear nature of the curve is clearly observed as predicted by Eq. (2), and very low deviation from the linear behavior is observed. A similar result is obtained for laser excitation. The inset of Fig. 4 also allows identifying that the actual magnitude of excited conductivity increases with temperature, as already mentioned. Unlike the evaluation done for undoped, Er-doped [9], and Eu-doped $SnO_2$ [19], where $\ln(slope/T) \times T^{-1}$ curve has negative inclination, the curves of Fig. 4 presents a positive inclination, which means that $(E_{cap} - \phi)$ presents a different behavior in the case of Sb-doped compared to rare-earth doped $SnO_2$. The value of $(E_{cap} - \phi)$ obtained from Fig. 4 is (−0.21 eV) for LED excitation and (−0.36 eV) for laser excitation. Although the barrier height is a function of temperature, using an average value of 0.7 eV [23] to estimate the value of $E_{cap}$, it is found 0.49 eV for LED excitation and 0.34 eV for laser excitation. In both cases, the value of $E_{cap}$ is lower than the barrier energy at grain boundary (0.7 eV), justifying the positive inclination in the curves of Fig. 4. The higher energy for the capture barrier obtained with the LED illumination can be explained as follows: the effect of shining light is the generation of a metastable state of high electronic density in the conduction band. It makes the Fermi level, which is already above the conduction band bottom (Fig. 1), to be raised to a higher level. The laser excites more electrons than the LED, due to the electron–hole excitation (absent with the LED excitation), besides the intrabandgap states (present in both illumination cases). Then, the Fermi level position in the laser excited sample is higher than the LED excited sample. As a consequence, the effective barrier seen by the metastably excited electrons is lower in the laser illumination case.

The Sb doping generates much shallower levels and must present a weakly temperature dependent trapping, because the sample is highly degenerated and the below bandgap light ionizes electrons to an already full conduction band. The overall consequence is a faster decay for lower temperatures and consequently, a positive slope in the linear variation of ln(*slope*/*T*) as function of $T^{-1}$. Thus, the value of $(E_{cap} - \phi)$ is always negative. Comparing the observed phenomena in Sb-doped $SnO_2$ with rare-earth doping $SnO_2$ thin films, one may state that the recombination process is much more energy consuming in the rare-earth doped compound, since $Er^{3+}$ and $Eu^{3+}$ acts as acceptors in this materials and then, having deeper energy levels.

## 5. Conclusion

All the striking behavior observed for photo induced conductivity decay of the Sb-doped $SnO_2$ thin film can be explained based on competing mechanisms: the capture process by thermally activated defects and the time–temperature variation of the mobility, which is dominated by the grain boundary scattering and decreases with temperature increase. From a theoretical data-fitting procedure, we conclude that although $Sb^{5+}$ related centers must present thermally activated capture cross section, this mechanism is overcame by the grain boundary scattering. The capture barrier ($E_{cap}$) shows a value lower than the potential barrier at grain boundary, independent on the energy of the irradiated light source. Then, the temperature dependency of trapping process is a much less sensitive than the mobility variation with temperature and time. Although the decay of photo excited conduction electrons is supposed to be faster for higher temperatures, the decay of the conductivity is faster for lower temperatures.

The understanding of photo-induced electrical properties of Sb-doped $SnO_2$ is essential toward a complete description of optoelectronic devices based on this material. Sb-doped $SnO_2$ thin films, deposited by sol–gel-dip-coating process, are rather resistive due to grain boundary scattering, even though the Sb doping increases the electronic density in the conduction band, because $Sb^{5+}$ acts as donors in this matrix.

## Acknowledgements

The authors wish to thank Dr. Evandro A. Morais for very fruitful discussions. They also acknowledge CNPq and FAPESP for financial support.

## References


[1] T.R. Giraldi, A.J.C. Lanfredi, M.T. Escote, E. Longo, J.A. Varela, C. Ribeiro, A.J. Chiquito, J. Appl. Phys. 102 (2007) 034312.
[2] T.D. Senguttuvan, L.K. Malhotra, Thin Solid Films (1996) 289.
[3] T. Rai, T.D. Senguttuvan, S.T. Lakshmikumar, Comput. Mater. Sci. 37 (2006) 15.
[4] C. Terrier, J.P. Chatelon, J.A. Roger, Thin Solid Films 95 (1997) 295.
[5] E.Kh. Shokr, M.M. Wakkad, H.A. Abd El_Ghanny, H.H. Ali, J. Phys. Chem. Solids 61 (2000) 75.
[6] A. Messad, J. Bruneaux, H. Cachet, M. Froment, J. Mater. Sci. 29 (1994) 5095.
[7] V. Geraldo, V. Briois, L.V.A. Scalvi, C.V. Santilli, J. Eur. Ceram. Soc. 27 (2007) 4265.
[8] V. Geraldo, V. Briois, L.V.A. Scalvi, C.V. Santilli, J. Phys. Chem. C 114 (2010) 19206.
[9] E.A. Morais, L.V.A. Scalvi, J. Eur. Ceram. Soc. 27 (2007) 3803.
[10] W.S. Cardoso, C. Longo, M.A. Paoli, Quim. Nova 28 (2005) 345.
[11] V. Geraldo, L.V.A. Scalvi, E.A. Moraes, C.V. Santilli, Mater. Res. 6 (2003) 451.
[12] R. Dovesi, V.R. Saunders, C. Roetti, R. Orlando, C.M. Zicovich-Wilson, F. Pascale, B. Civalleri, K. Doll, N.M. Harrison, I.J. Bush, Ph. D'Arco, M. Llumel, 2006 CRYSTAL03 User's Manual, University of Torino.
[13] W. Khon, A.D. Becke, R.G. Parr, J. Phys. Chem. 100 (1996) 12974.
[14] C. Lee, W. Yang, R.G. Parr, Phys. Rev. B 37 (1988) 785.
[15] J.R. Sambrano, G.F. Nóbrega, C.A. Taft, J. Andrés, A. Beltrán, Surf. Sci. 580 (2005) 71–79.
[16] K.L. Schuchardt, B.T. Didier, T. Elsethagen, L. Sun, V. Gurumoorthi, J. Chase, J. Li, J. Chem. Inf. Model. 47 (2007) 1045.
[17] Theory of Condensed Matter Group, Antimony Basis Sets for the Crystal Program, http://www.tcm.phy.cam.ac.uk/~mdt26/basis_sets/Sb_basis.txt (accessed 05.01.11).
[18] S. Munnix, M. Schmeits, Phys. Rev. B 27 (1983) 7624.
[19] E.A. Morais, L.V.A. Scalvi, A.A. Cavalheiro, A. Tabata, J.B.B. Oliveira, J. Non-Cryst. Solids 354 (2008) 4840.
[20] E.A. Morais, L.V.A. Scalvi, V. Geraldo, R.M.F. Scalvi, S.J.L. Ribeiro, C.V. Santilli, S.H. Pulcinelli, J. Eur. Ceram. Soc. 24 (2004) 1857.
[21] T.W. Dobson, L.V.A. Scalvi, J.F. Wager, J. Appl. Phys. 68 (1990) 601.
[22] D.H. Zhang, H.L. Ma, Appl. Phys. A 62 (1996) 487.
[23] M.A.L. Pinheiro, T.J. Pineiz, E.A. Morais, L.V.A. Scalvi, M.J. Saeki, A.A. Cavalheiro, Thin Solid Films 517 (2008).